Chemical Geology 537 (2020) 119474

Contents lists available at ScienceDirect

Chemical Geology

journal homepage: www.elsevier.com/locate/chemgeo

Origins of high $\delta^{18}O$ in 3.7–3.6 Ga crust: A zircon and garnet record in Isua clastic metasedimentary rocks

Laure Gauthiez-Putallaz[a,*], Allen Nutman[b], Vickie Bennett[a], Daniela Rubatto[a,c]

[a] Research School of Earth Sciences, Australian National University, Canberra 2601, ACT, Australia
[b] School of Earth, Atmospheric and Life Sciences, University of Wollongong, NSW 2522, Australia
[c] Institute of Geological Sciences, University of Bern, CH-3012, Switzerland

ARTICLE INFO

Editor: Catherine Chauvel

Keywords:
Eoarchean
Weathering
Oxygen Isotopes
SHRIMP
Isua
Metasediments

ABSTRACT

Elevated $\delta^{18}O$ is used as a marker for the presence of continents and surficial alteration in the Eoarchean and Hadean. This study establishes a timeline for $\delta^{18}O$ enrichment in Eoarchean metasedimentary rocks of the Isua supracrustal belt in Greenland. The source-rocks for the protolith of these metasedimentary rocks are mafic to intermediate magmatic rocks of $\geq 3709 \pm 4$ Ma, based on the age of zircons found in volcanogenic layers. The $\delta^{18}O$ of $+5.4 \pm 0.4$‰ of the zircon crystals indicate that the sources had a primary mantle-derived signature. However, garnet in two metasediments yields higher $\delta^{18}O$ values of $+8.7$ to $+9.7$‰, in equilibrium with a whole-rock of $+11$ to $+12$‰ at 500–600 °C. This requires that the mafic protolith was weathered at surficial conditions, in agreement with previous conclusions based on major element geochemistry. The garnet grains with high $\delta^{18}O$ record four growth zones, assigned to I) arc-building thermal metamorphism, II–III) terrane assembly at medium to high-pressure conditions, estimated to occur at 3660–3690 Ma and IV) late-Archaean overprint likely at ca. 2690 Ma. This shows that material with originally mantle-like $\delta^{18}O$ was altered at low temperature (near-surface) to generate elevated oxygen isotope signatures and then recycled to middle-crustal conditions within 10–50 million years of crystallization in the Eoarchean. We propose that melting of such rocks could produce the zircon crystals with high $\delta^{18}O$ that are found in the detrital and magmatic record in the Archean.

1. Introduction

The emergence of continents and their interactions with the ocean and atmosphere in the early Earth is key to understanding early life and plate tectonics. Geochemical signatures of relict Eoarchean minerals and rocks offer precious clues about these early events. Among them, oxygen isotopes have been used as a tracer for surficial processes, as the strongest oxygen isotope fractionation occurs by fluid-rock interaction at low temperature (e.g. Lawrence and Taylor, 1971; Gregory and Taylor, 1981). Notably, the discovery of high $\delta^{18}O > 6$‰ in Hadean zircons yielded the first evidence for early crust formation involving a hydrosphere (e.g. Wilde et al., 2001; Mojzsis et al., 2001; Trail et al., 2007). This study focuses on novel evidence for Eoarchaean weathering processes in the Isua supracrustal belt at ca. 3700 Ma, creating heavy oxygen isotope signatures in the protoliths of metasedimentary rocks prior to metamorphism in the Eoarchean.

In order to track protolith signatures and reconstruct multiple stages in the evolution of ancient rocks it is necessary to investigate robust and refractive minerals. In this study, in situ measurement of oxygen isotopes by ion microprobe (SHRIMP) in magmatic zircon and garnet is used to track how the $\delta^{18}O$ signature changed from the source to the sediment and throughout metamorphism. Garnet in particular has the capacity to record multiple stages of metamorphism during crustal thickening and collision. Such complex garnet zoning has been described in metasedimentary rocks from the Isua supracrustal belt (Rollinson, 2002, 2003) that record a multi-phased metamorphic history, starting potentially as early as 3700 Ma (Blichert-Toft and Frei, 2001). Like zircon, garnet can retain primary oxygen isotope signatures up to high temperatures (e.g. Vielzeuf et al., 2005; Higashino et al., 2019). Similarly to previous studies of this type in Phanerozoic metamorphic terranes (e.g. Martin et al., 2014; Page et al., 2014; Rubatto and Angiboust, 2015), petrography and garnet chemistry are used to link $\delta^{18}O$ signatures to tectonic events. The inferred protolith signatures are compared to other regional values in order to investigate the degree of surface alteration in Eoarchean sedimentation processes. The $\delta^{18}O$ data are used to establish if any important fluid circulation or

* Corresponding author.
E-mail address: laure.gauthiez-putallaz@anu.edu.au (L. Gauthiez-Putallaz).

https://doi.org/10.1016/j.chemgeo.2020.119474
Received 2 June 2019; Received in revised form 15 December 2019; Accepted 16 January 2020
Available online 17 January 2020
0009-2541/ © 2020 Elsevier B.V. All rights reserved.

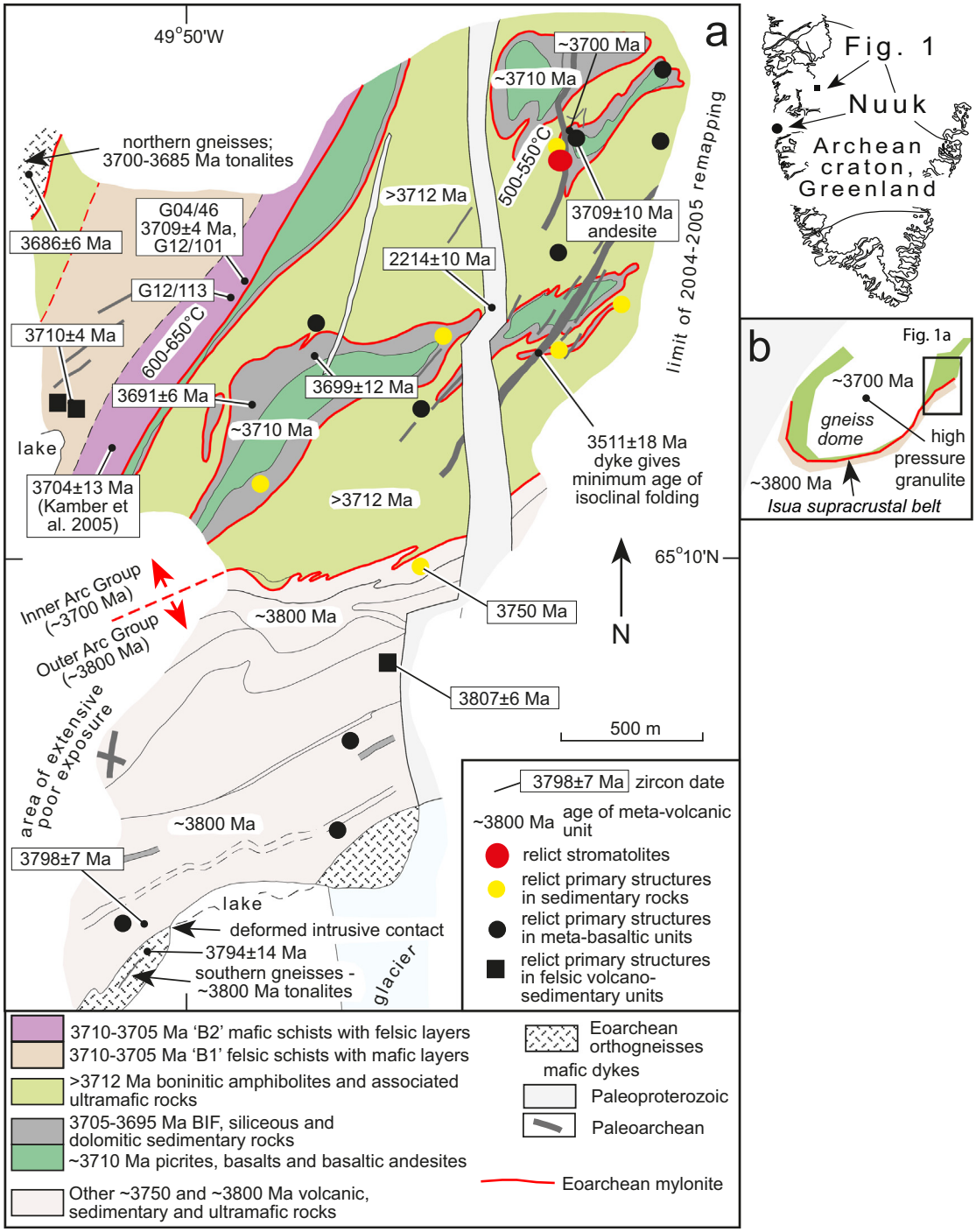

Fig. 1. (a) Tectonic map of the eastern part of the Isua Supracrustal Belt (modified from Nutman and Friend, 2009) with previously obtained zircon ages, (b) Overview of the Isua Supracrustal Belt.

metasomatism affected these rocks during metamorphism. Finally, we examine the consequences for the recycling of surficial signatures in the early Earth's crust.

1.1. Geologic context

Owing to the exceptional preservation of a variety of surficial lithologies and of their contact relationships, the Isua supracrustal belt (Fig. 1) is unique for the study of the early Earth. Following half a century of research, it has been subdivided into multiple tectonic, geochemical and metamorphic packages (e.g. Nutman et al., 1997; Rollinson, 2002; Nutman and Friend, 2009; Fig. 1), which are considered to represent different structural levels of two proto-arcs formed at about 3700 Ma and 3800 Ma (e.g. Nutman et al., 2015a). In this study, we focus on a unit known as the B2 unit (Nutman et al., 1984) of predominantly mafic and lesser felsic metasedimentary schists from the NE part of the Isua supracrustal belt which is part of the 3700 Ma package of Nutman and Friend (2009; Inner Arc Group on Fig. 1a), *northwestern tectonic package* of Appel et al. (1998) and *domain II* of Rollinson (2002, 2003). This sedimentary assemblage has been interpreted by Nutman et al. (2015a, 2017) as an arc-related volcano-sedimentary package, consisting of the distal facies of turbidites, derived from andesitic material (Rosing, 1999; Bolhar et al., 2004; Bolhar et al., 2005) and deposited into mafic-derived mudstones. The age of

the sedimentary protolith is ca. 3705 Ma from sparse zircon dates obtained from four samples (Nutman et al., 1997; Nutman and Friend, 2009; Kamber et al., 2005).

Recent whole-rock studies by Nutman et al. (2015b, 2017, 2019), report high-$\delta^{18}O$ lithologies that are interpreted as the result of Eoarchean low-temperature alteration in the Isua supracrustal belt. High-$\delta^{18}O$ metasedimentary rocks were discovered in the ca. 3700 Ma package. In particular, in the *Central tectonic domain* were identified potential weathered surfaces of andesitic compositions with values of ca. +16‰, as well as other metasedimentary rocks, including the B2 schists (values of ca. 12‰, Nutman et al., 2017). Significantly, felsic schists from the ca. 3800 Ma domain were reported to contain mantle-signature zircons of magmatic origin and WR $\delta^{18}O$ of 14.6 to 16.2‰ (Nutman et al., 2015a; Hiess et al., 2009), and interpreted as felsic volcanic rocks altered at low-temperature. This study aims at assessing when the B2 schists acquired their high-^{18}O signature and how it evolved during Eoarchean higher-pressure metamorphism.

Previous detailed studies have shown that the Isua metasedimentary rocks have a multi-phased metamorphic history, starting potentially as early as 3700 Ma (Blichert-Toft and Frei, 2001). Staurolite and kyanite-bearing assemblages were first recognized by Boak and Dymek (1982), and they indicate a Barrovian-style event at about 600–650 °C and 6 kbar. This event was also recognized by Rollinson (2002, 2003) as a Ca-rich annulus present in garnets from the B2 unit. This metamorphic event is unique to the 3700 Ma package Domain II of Rollinson (2002, 2003), and is not recognized in the ~3800 Ma Outer Arc Group package (Fig. 1a) of the Isua supracrustal belt.

The B2 unit was intruded by the ~3500 Ma Ameralik dykes a suite of dolerites and norites (McGregor, 1973; Nutman et al., 2004; Fig. 1b). Throughout the Isua area, the Ameralik dykes are weakly deformed to undeformed, and display epidote-amphibolite facies metamorphic assemblages (e.g., Nutman, 1986; Rollinson, 2002). This uniform regional epidote-amphibolite facies metamorphism predates undeformed mafic dykes intruded at 2214 ± 10 Ma (Nutman et al., 1995; Fig. 1), and probably occurred in the Neoarchean at ~2690 Ma (Nutman and Collerson, 1991). The Ameralik dykes have metamorphic assemblages that indicating uniform Neoarchean P-T conditions and cut tectonic panels of Eoarchean rocks with *different* metamorphic histories (e.g., Rollinson, 2003). This association demonstrates a complex pattern of Eoarchean, pre-3500 Ma metamorphism in the Isua supracrustal rocks.

Structurally deeper than the B2 schists, in the refolded gneiss dome north of the Isua supracrustal belt (Fig. 1b), there are rare relicts of 3658 ± 3 Ma, > 700 °C high pressure granulite assemblages (grt + cpx + pl + qz + hbl + ttn, mineral abbreviations are from Whitney and Evans, 2010) in mafic rocks, which are interpreted, together with the Barrovian-style metamorphism in the B2 schists, as the result of an episode of crustal thickening (Nutman et al., 2013). The high pressure granulite assemblages are in enclaves overprinted by voluminous sheets of 3650–3630 crustally-derived anatectic granites and pegmatites which were emplaced in an extensional regime (Nutman and Bridgwater, 1986; Nutman et al., 2000; Crowley and Myers, 2002). To the south and east of the B2 unit, peak metamorphic conditions are lowest, with maximum temperature of 500–550 °C (Fig. 1a; Rollinson, 2003). The domains with the high pressure granulite facies relicts, B2 unit with Barrovian assemblages and the lowest metamorphic grade rocks to the southeast are now horizontally ≤10 km apart, and are partitioned by pre-Ameralik dyke shear zones (Eoarchean mylonites, Fig. 1a). These domains units are interpreted as the centre and margins respectively of an Eoarchean core complex, developed during recovery and extension in the previously thickened crust (Nutman et al., 2013). 3660–3650 Ma anatectic granite sheets are present in both the 3700 Ma Inner Arc group and the 3800 Ma Outer Arc group, which give a minimum age constraint for the crustal thickening event that intervened early in the assembly of the two groups (Crowley, 2003; Nutman et al., 2014). The B2 schists thus represent a rare record of the early metamorphic history of the Isua Supracrustal belt, starting from Barrovian-style crustal thickening event pre-3650 Ma.

2. Methods

Whole rock (WR) powders were obtained by agate mill grinding. Major elements were measured on fused discs at Geoscience Australia (GA). Fused discs were produced using an Initiative Scientific Products Fusilux 4 × 4 Fusion Machine using a proportion of 6.000 g of flux for 1.000 g of sample, fusing at 1100 °C for 10 min in platinum crucibles. X-ray flux 12:22 (35.3% $Li_2B_4O_7$ - tetraborate, 64.7% $LiBO_2$ – metaborate) was used. The flux is certified containing 0–1 ppm of Pb, Ni, Mn, Cd, Zn, Co, Ag; 1–5 ppm K, Cu, Se, As, Al, Sn, Na, Fe; 2–10 ppm Si, S, Ca and Mg. Powder aliquots were measured on a C/H/moisture analyser Leco RC-612 at GA. Fused discs were recovered from XRF analysis, mounted in epoxy disks, cut in their centre and polished. Whole rock (WR) trace elements were measured the Research School of Earth Sciences (RSES) at the Australian National University (ANU) using an ArF excimer laser coupled to a quadrupole Inductively Coupled Plasma Mass Spectrometer (ICP-MS) Agilent 7700. The laser was tuned to a frequency of 5 Hz and energy of 50 mJ (corresponding to a HV of around 26–27 kV). The spot size was set to 103 μm. Background was measured for 20 s before 45 s analysis. Calcium, previously determined by XRF, was used as an internal standard. The reported values are the average of 3 spots in the same glass disk. NIST 610 and 612 were used for high (> 100 ppm) and low-concentration elements respectively and the BCR basalt (USGS) was used as a secondary standard. Reproducibility and accuracy as assessed on the BCR-2G glass were within 10% or less for all analysed elements. XRF and LA-ICP-MS concentrations were within ± 10% of each other for elements V, Zn, Rb, and Zr. The data were reduced with the software Iolite (Paton et al., 2011) using the data-reduction scheme for trace elements (Woodhead et al., 2007), followed by an additional step of standardising to the Ca content of the samples.

Back-scattered electron (BSE) and secondary electron (SE) investigation of garnet in thin section, as well as Cathodoluminescence (CL) of zircon, were carried out on a JEOL JSM-6610A scanning electron microscope (SEM) at the RSES. Operating conditions for the SEM were 15 kV, a load current of 65–75 μ A and a 10–12 mm working distance. Spot qualitative major element analyses were obtained with a solidstate Energy Dispersive (EDS) detector on the same JEOL instrument, using an acceleration voltage of 15 kV and a current of 60–70 nA. Analyses were checked for stoichiometry; analyses of UWG2 garnet were within 5% of EMPA analyses on the same UWG2 batch and published values (Valley et al., 1995). X-ray compositional maps were acquired by electron probe micro-analyser (EPMA) in wavelength-dispersive mode. EPMA analyses were carried out with a JEOL JXA-8200 superprobe at the Institute of Geological Sciences (University of Bern). Compositional maps were acquired following the procedure described in Lanari et al. (2012, 2013) using 15 kV accelerating voltage, 100 nA beam current and dwell times of 200 ms. The element maps were acquired with a step size of 6 μm. The compositional maps were classified and converted into maps of garnet endmembers on a 12 oxygen basis using the software XMapTools 2.3.1 (Lanari et al., 2014).

Zircon and garnet trace elements were measured by Laser Ablation ICP-MS at RSES at the conditions described above for WR. Spot sizes of 22 and 28 μm for zircon and of 62 μm for garnet were used. Data were acquired over a 65 s analysis that included a 20 s background. Analyses were standardised to NIST 610 (zircon) and NIST 612 (garnet) glasses. Values of Spandler et al. (2011) have been used for data reduction. Stoichiometric Si was employed as internal standard for zircon (SiO_2: 31.6 wt%) and garnet (SiO_2: 42 wt%). Reproducibility and accuracy as assessed on the BCR-2G glass were within ± 10% or less for all analysed elements. The data were reduced with the software Iolite (Paton et al., 2011) and its data-reduction scheme for trace elements (Woodhead et al., 2007).

Zircon oxygen isotopes were analysed on the same mounts as used

for U–Pb dating with the SHRIMP II instrument at ANU, after a short re-polish and subsequent re-coating, following the analytical procedure described in Ickert et al. (2008). All $\delta^{18}O$ values are reported relative to Vienna Standard Mean Oceanic Water – VSMOW. The standard Temora2 ($\delta^{18}O$ = 8.2‰, Black et al. 2004, Avila et al. 2019) was used. The repeatability of Temora2 zircon was within 0.5‰ (2σ) during each analytical session. Garnet oxygen isotopes were measured on SHRIMP II and SHRIMP SI at ANU following the method of Martin et al. (2014), and correcting for instrument mass fractionation and compositional bias. The value of the standard garnet UWG2 (5.8‰, Valley et al., 1995) was reproduced within 0.3‰ (2σ) in each analytical session. Analyses of garnet and zircon consisted of 5 scans of 20 s for a total counting time of 100 s. Raw data were processed with the in-house software POXI-MC. For garnet, a matrix correction for grossular content was made according to calibrations by Martin et al. (2014) acquired in the same year as the unknown analyses, with similar tuning and running parameters. Garnet chemistry was acquired by EDS analysis, measured a posteriori next to each SHRIMP spot. Error propagation for oxygen isotope analyses follows Martin et al. (2014).

Zircon U–Pb dating was performed on the SHRIMP II at ANU, using a setup modified from Williams (1998). Standards and unknowns were analysed with a spot size of around 20 by 25 μm. Temora2 zircon (U–Pb age of 417 ± 1 Ma, Black et al. 2003) was used as standard for instrumental U–Pb mass fractionation and U concentration (160 ppm). The calibration error during the analytical sessions was 1.5% and this uncertainty was propagated in quadrature to individual analyses. Ratios were corrected for common Pb according to the measured $^{204}Pb/^{206}Pb$ ($^{4/6}R_m$) and the non-radiogenic $^{204}Pb/^{206}Pb$ ($^{4/6}R_c$) following the method described in Williams (1998), i.e. $f_{206} = {}^{4/6}R_m/{}^{4/6}R_c$. The $^{4/6}R_c$ composition was assumed to be that predicted by Stacey and Kramers (1975) model. Most analyses yield < 1% common ^{206}Pb, so the choice of the common Pb model has no significant impact on the ages. Data reduction and assessment was performed using MS Excel extensions SQUID 2.5 (Ludwig, 2009) and Isoplot 4 (Ludwig, 2012).

3. Results

3.1. Sample petrography

The B2 unit (Nutman et al., 1984, 1997), outcrops as an extensive sequence of layered biotite-chlorite-garnet schists over ca. 5 km along strike. Most layers are coarse-grained with cm-sized garnets embedded in a matrix of chlorite with quartz layers, and quartz and calcite veinlets. Many layers contain pale-blue pseudomorphs made of finely grained white mica interspersed with staurolite relicts and chloritoid. Kyanite was found in samples of the same unit by Boak and Dymek (1982) but was not observed in this study. Two mafic schist samples (G12/101, G12/113) were studied in detail for thin section petrography and garnet zoning (Table 1). Zircon grains from a more felsic sample (G04/46) were used for U–Pb dating and oxygen isotope analysis.

G12/101 is a fine layered plagioclase-chlorite-garnet-quartz-tourmaline schist with 5–10 mm garnet crystals (Fig. 2); G12/113 is a more quartz-rich garnet-chlorite rock with minor tourmaline and numerous staurolite relicts and pseudomorphs after staurolite (Fig. 2, Fig. 3a). Some of these staurolite pseudomorphs contain chloritoid needles that grew over staurolite relicts, statically over the main foliation. In both samples, garnet shows rotational structures compared to the main foliation (Fig. 3b).

G04–46 is a layered felsic gneiss in which biotite and chlorite-rich layers contain more garnet than quartz-rich layers. In quartz-rich layers, garnet grows in a skeletal texture, which impedes the interpretation of outwards growth zoning. Small (ca. 200 μm) garnet crystals in the chlorite-rich layers yield concentric zoning that is similar to what is observed in the chlorite schists G12-113 and G12-101 (Fig. 2c, d).

3.2. Whole Rock Geochemistry

Sample G12/101 and G12/113 are mafic to intermediate in composition (51.7 and 60.9 wt% SiO_2, Table 2), they are both rich in Al_2O_3 and Fe_2O_3, but G12/113 is much poorer in alkalis than G12/101. Gneiss G04/46, from which the zircon crystals were separated, is more felsic with 75.6 wt% SiO_2.

Mafic schists G12/101 and G12/113 have parallel trace element patterns that are enriched in incompatible elements compared to the primitive mantle (Fig. 4a). Both samples have a marked negative Nb–Ta anomaly, a positive Zr–Hf anomaly and slight positive Eu and Sr anomalies.

Felsic layer G04/46 is enriched in incompatible elements (Fig. 4b) but with marked negative anomalies in Ba, Nb–Ta, Sr, Eu and Ti. The anomalies imply the fractionation of plagioclase and a Ti phase, which is also typical of other Isua dioritic and tonalite rocks of equivalent age (e.g. Nutman et al., 2013).

Aliquots of the G04/46, G12/101 and G12/113 whole-rock powders were analysed for $\delta^{18}O$ using the conventional fluorination technique (data reported in Nutman et al., 2017, method described in Nutman et al., 2015a) and yielded values between +11.8 and +13.0‰, with an analytical uncertainty is 0.1‰ (1σ). Repeated analysis of samples G12/101 and G12/113 after further hand-crushing yielded slightly lower $\delta^{18}O$ value of +11.5 and +11.6‰, respectively.

3.3. Zircon geochronology and geochemistry

Sparse, small prismatic zircon crystals were recovered from sample G04/46. They are mostly oscillatory zoned (Fig. 5a), which is a common feature of magmatic zircons (e.g. Hoskin and Schaltegger, 2003). The zircon oscillatory-zoned cores display embayments and very narrow (< 10 μm) overgrowths that are bright in CL and that could not be analysed in sectioned crystals because of their small size. It is speculated that the overgrowths indicate a fluid related dissolution-reprecipitation event, probably during metamorphism. Oscillatory-zoned domains in G04/46 zircon crystals yield a weighted mean $^{207}Pb/^{206}Pb$ age of 3709 ± 4 Ma (MSWD = 1.2, 11 analyses) and a Concordia age of 3709 ± 6 Ma (95% confidence level; Fig. 5a,b; Supplementary material 1). These domains have Th/U between 0.6 and 1.1, typical of intermediate to mafic igneous zircon (e.g. Hoskin and Schaltegger, 2003). The common Pb content of the analyses is below 1% in all cases.

The REE pattern of the oscillatory zones shows a negative Eu anomaly and a positive Ce anomaly, together with strong HREE enrichment. The patterns are similar to what is documented for Phanerozoic magmatic zircons (e.g. Hoskin and Schaltegger, 2003; Fig. 5 c, Supplementary material 2). Oxygen isotopes were measured in oscillatory-zoned zircon grains (Fig. 6a, Supplementary material 3). The results return a homogenous population of typical mantle $\delta^{18}O$ value at

Table 1
Sample characteristics. Mineral abbreviations are from Whitney and Evans (2010).

Sample #	Rocktype	Area	Latitude	Longitude	Mineralogy	Facies
G12/101	Chlorite-garnet schist	Isua	65°10′26.5″	49°49′40.2″	Chl, Grt, Qz, Ms., Pl, Tur, Ilm, Cal	Amphibolite
G12/113	Garnet-chlorite fels	Isua	65°10′18.6″	49°49′58.6″	Chl, Grt, Qz, Ms., St, Cld, Tur, Ilm	Amphibolite
G04/46	Plagioclase-amphibole gneiss	Isua	65°10′26.5″	49°49′40.2″	Qz, Pl, Bt, Chl, Grt, Ilm, Zrn	Amphibolite

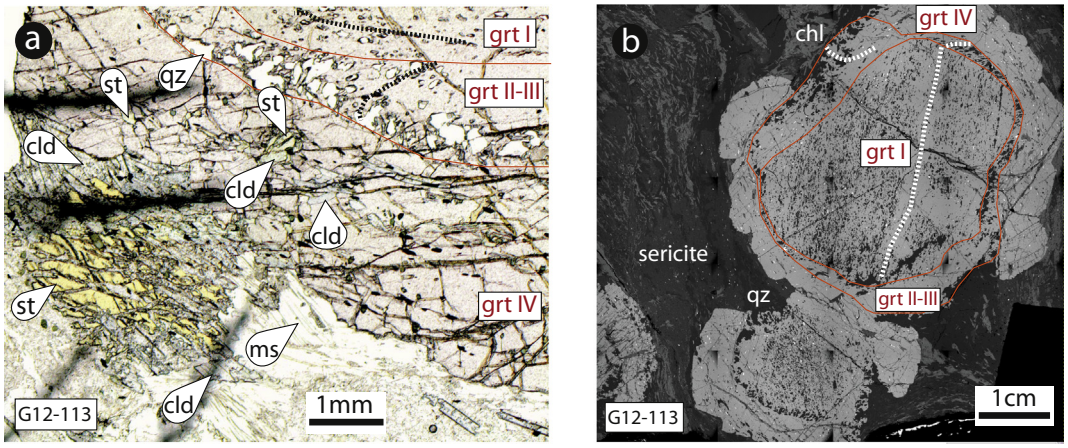

Fig. 2. Thin-section optical scan showing the microtexture of samples G12/101 (a) and G12/113 (b). In G12/113, the dotted lines outline staurolite pseudomorphs and the arrows indicate staurolite relicts. (c) Secondary-electron image of a quartz-rich layer showing the mineral distribution. (d) BSE image of a garnet grain in sample G04/46 showing chemical zoning.

+5.4 ± 0.4‰ (1sd, n = 20). One zircon as inclusion within a garnet was analysed in situ and also yields a mantle-like value of +6.0‰ (Fig. 6b). One single zircon rim in a fractured grain yields a distinctly higher $\delta^{18}O$ of 10.1 ± 0.1‰ (1SE).

3.4. Garnet geochemistry

Typical garnet crystals in both samples (8 mm across in sample G12/101 and 15 mm across in G12/113) show a zoning pattern consisting of 4 distinct zones from core to rim that are identified on the basis of texture and major elements (Fig. 3b, Fig. 7, Supplementary material 4, 5). Generally, Mn decreases ($Sps_{0–18}$) and Mg increases ($Alm_{68–88}$) from core to rim, and sharp changes in Ca content mark the zones. Zone I defines the garnet core, and is relatively rich in Mn and poor in Ca (G12/101-*I*: $Prp_{4–5}$, $Grs_{8–9}$, $Sps_{13–19}$, $Alm_{68–73;}$ G12/113-*I*: $Prp_{4–5}$, $Grs_{5–7}$, $Sps_{9–18}$, $Alm_{72–81}$); the Mn concentration has a slight bell-shaped profile from the inner to the outer part of the core. In sample G12/113, this zone yields numerous quartz inclusions that define an internal foliation (Fig. 3b). Zone II is marked by a sharp increase in Ca that then decreases outwards, and a gradual decrease in Mn (G12/101-*II*: $Prp_{4–5}$, $Grs_{15–21}$, $Sps_{8–14}$, $Alm_{64–72;}$ G12/113-*II*: $Prp_{4–5}$, $Grs_{8–11}$, $Sps_{6–8}$, $Alm_{79–81}$). This zone contains larger inclusions. Zone III is again marked by sharp increase in but with even lower Mn content (G12/101-*III*: $Prp_{4–6}$, $Grs_{19–21}$, $Sps_{1–5}$, $Alm_{71–73;}$ G12/113-*III*: $Prp_{4–6}$, $Grs_{7–16}$, $Sps_{1–5}$, $Alm_{77–85}$). Zone IV is the outer rim and is characterised by another sharp change in Ca to low concentrations comparable to the core, and by the highest Mg content (G12/101-*IV*: $Prp_{6–9}$, $Grs_{5–12}$, $Sps_{0–4}$, $Alm_{79–85;}$ G12/113-*IV*: $Prp_{6–10}$, $Grs_{3–8}$, $Sps_{0–1}$, $Alm_{85–88}$).

The sharp boundaries observed between the core and Zone II as well as between Zone II and III in G12/101 (Fig. 7a) are underlined by the presence of μm-sized mineral and fluid inclusions. Ilmenite, rutile, plagioclase, quartz, tourmaline and chlorite are inclusions in zone I of garnet G12/113. In zone II, rutile, ilmenite, tourmaline and quartz were found. Zone III yields tourmaline and ilmenite, while rutile can be

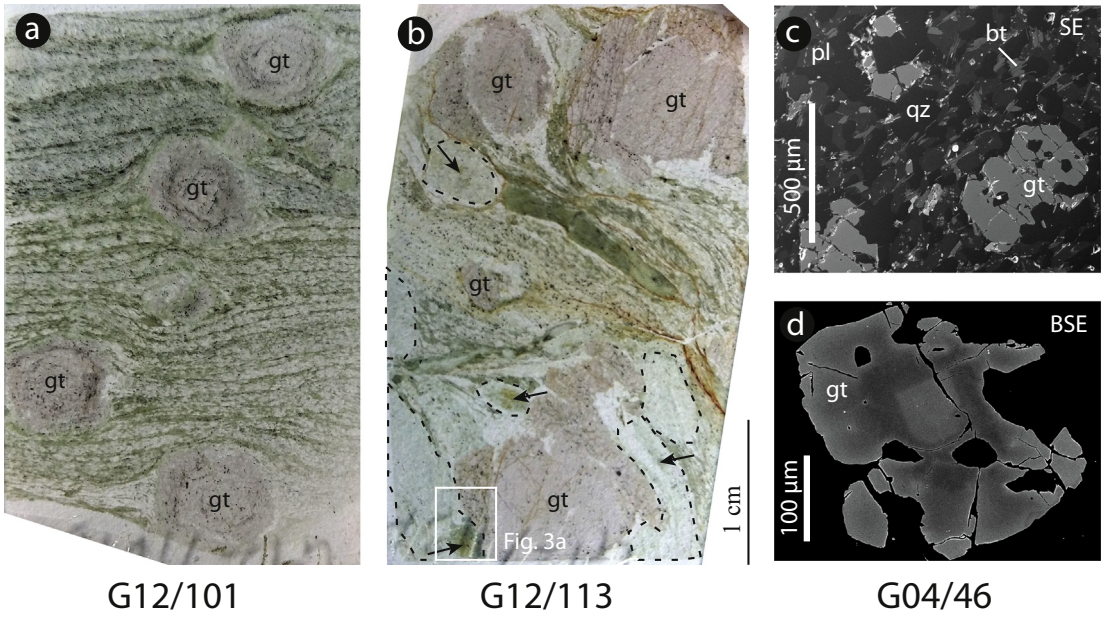

Fig. 3. (a) G12/113 transmitted light photomicrograph of matrix and garnet inclusion mineralogy: Garnet Zone IV (grt IV) contains inclusion of relict staurolite and of chloritoid. Garnet Zones I to IV correspond to chemical zones described in text. (b) G12/113 Back-scattered-electron image of two garnet grains showing the rotation of inclusion trails (dotted lines) and the textural relationship between zones (red lines). (For interpretation of the references to colour in this figure legend, the reader is referred to the web version of this article.)

Table 2
XRF Major and LA-ICP-MS trace element composition of Isua samples.

	G04/46	G12/101	G12/113
		chl-grt-qz-pl-tur	chl-grt-qz-st
XRF (wt%)			
SiO_2	75.6	51.7	60.9
Al_2O_3	10.1	20.5	16.0
Fe_2O_3	6.9	13.0	13.4
MnO	0.1	0.2	0.7
MgO	2.6	4.1	2.2
CaO	1.5	2.4	1.1
Na_2O	1.3	3.2	1.7
K_2O	0.7	1.3	1.2
P_2O_5	bdl	bdl	bdl
TiO_2	0.2	0.4	0.4
XRF sum	98.9	96.7	97.6
H_2O (LECO wt%)	2.0	3.7	2.1
CO_2 (LECO wt%)	0.2	0.7	0.1
Total sum	101.3	101.3	100.0
Nutman et al., 2017			
$\delta^{18}O_{VSMOW}$ (‰)	+13.0 (+13.0)	+11.6 (+11.8)	+11.5 (+12.6)
LA-ICP-MS (μg/g)			
Sc	12.3	45.4	43.5
Ti	1083	2341	2325
V	29.0	204	138
Cr	76.1	1033	726
Mn	500	1369	4751
Co	14.5	60.0	36.9
Ni	47.3	434	185
Cu	3.5	5.5	41.7
Zn	38.0	96.5	28.9
Ga	14.8	23.4	17.3
Ge	11.0	7.6	13.0
Rb	39.6	39.7	39.7
Sr	66.5	132	66.6
Y	18.3	9.1	14.5
Zr	152	49.9	68.9
Nb	5.9	1.4	1.9
Cs	0.9	0.4	0.4
Ba	57.6	198	137
La	27.2	4.7	3.2
Ce	56.0	9.2	6.5
Pr	6.4	1.1	0.8
Nd	24.6	4.7	3.3
Sm	4.6	1.1	1.0
Eu	0.7	0.5	0.5
Gd	3.8	1.2	1.5
Tb	0.6	0.2	0.3
Dy	3.3	1.5	1.9
Ho	0.6	0.3	0.4
Er	1.9	1.1	1.6
Tm	0.3	0.2	0.3
Yb	1.8	1.1	1.8
Lu	0.2	0.2	0.3
Hf	4.5	1.3	2.0
Ta	0.5	0.1	0.1
W	0.5	1.3	0.6
Pb	7.3	14.5	8.4
Th	6.2	0.9	1.4
U	1.0	0.1	0.3

observed in cracks. Zone IV is generally inclusion-poor, but in one instance, it contains composite inclusions of staurolite and chloritoid (Fig. 3a), similar to pseudomorphs observed in the matrix.

In both samples, the garnet core (Zone I) is the most enriched in HREE (Fig. 7d, Supplementary material–6), with a gradual depletion towards the outer core similar to what is observed for Mn, a proxy of Rayleigh fractionation during garnet growth. This fractionation trend results in a change in HREE concentrations of two orders of magnitude in sample G12/113 that contains large garnet grains. Zone I yields a marked Eu anomaly in both samples, which is indicative for the presence of plagioclase in the co-existing assemblage because neither of these samples shows negative Eu anomalies in their whole-rock composition (Fig. 4). Zone II and zone III display no Eu anomalies in both samples, which suggests that plagioclase reacted out or significantly decreased in abundance during this stage. The HREE content of these garnet zones is generally lower than Zone I, indicating that most HREE were fractionated in the garnet cores. Zone IV yields different REE signatures in the two samples. In sample G12/113, Zone IV yields a small to negligible negative Eu anomaly; this is in line with only minor plagioclase in the matrix, which is and restricted to thin layers (mode ca. 0.5–1%). Particularly in sample G12/113 that contains large garnet grains, Zone II and IV have extreme depletion in M-HREE, which is interpreted as an effect of the fractionation of HREE in the inner garnet zones. In sample G12/101, the garnet rim yields a marked negative Eu anomaly and this is correlated to the presence of plagioclase in the matrix (mode ca. 40%).

G04/46 is a layered felsic rock in which amphibole and chlorite-rich layers contain more garnet than quartz-rich layers. In quartz-rich layers, garnet grows in a skeletal texture that impedes the interpretation of outwards growth zoning. Garnet in the amphibole-rich layers yields concentric zoning that is similar to what is observed in the schists G12/113 and G12/101.

Oxygen isotope analyses were performed in each zone along two core-rim profiles in garnet G12/113 (length of profile: 7 mm). In addition, a third and more detailed profile of the garnet mantle was measured (Fig. 8, Supplementary material 7). In garnet G12/113, the core yields an average $\delta^{18}O$ of +9.2 ± 0.1‰ (1sd, n = 11), Zone II +9.7 ± 0.3‰ (1sd, n = 5), zone III +9.4 ± 0.2‰ (1sd, n = 19) and zone IV 8.7 ± 0.3‰ (1sd, n = 15). The total uncertainty for these averages calculated following the procedure of Martin et al. (2014) is in the range of 0.5–0.6‰ (2σ), and is dominated by the grossular and spessartine matrix calibration uncertainty. For consistency, both grossular and spessartine corrections were applied in all measurements, even though the correction for spessartine is negligible for zone III and IV compositions.

Similarly, two rim–core profiles were measured in garnet G12/101 (length 4 mm, Fig. 8). In this smaller garnet, less variation is observed from core to rim, from a $\delta^{18}O$ of +9.4 ± 0.2 (1sd, n = 8) in the core (zone I), Zone II +9.4 ± 0.2‰ (1sd, n = 6), zone III +9.7 ± 0.1‰ (1sd, n = 4), to a value of +9.3 ± 0.2 (1sd, n = 13) in the external rim (IV).

4. Discussion

4.1. Sedimentary source of the Isua B2 schists

From major and trace element data, it has been inferred that the B2 schists are predominantly derived from mafic sources (Dymek et al., 1983; Nutman et al., 1984; Bolhar et al., 2005). The two schists investigated here are comparable in trace element composition to the more mafic rocks in Nutman et al. (2013), more specifically boninites and basalts(Fig. 4).The high contents in Cr and Ni in samples G12/101 and G12/113 are in line with a protolith rich in mafic minerals such as olivine, clinopyroxene and spinel. The contribution of mafic sources derived from depleted mantle, such as Isua supracrustal belt ≥3710 Ma boninites and basalts, was specifically proposed by Polat et al. (2002) and Nutman et al. (2015a). The trace element composition of G12/101 and G12/113 have strong similarities to the samples with positive Eu anomalies identified by Bolhar et al. (2005), which the author interpreted as clastic sediments derived from mafic sources, for which the Eu anomaly was developed because of precipitation of marine Fe-oxyhydroxides during deposition or diagenesis.

The trace element pattern of felsic rock G04/46 (Fig. 4) is similar to felsic volcanogenic samples in Bolhar et al. (2005) and fresh ca. 3710 Ma andesites (Nutman et al., 2013). The high-SiO_2 content of the felsic layer is not due to later silica veining, because the unit is uniformly fine-grained. Instead it is likely due to silification of a volcanic layer at the surface – a process widespread in Archean volcanic rocks.

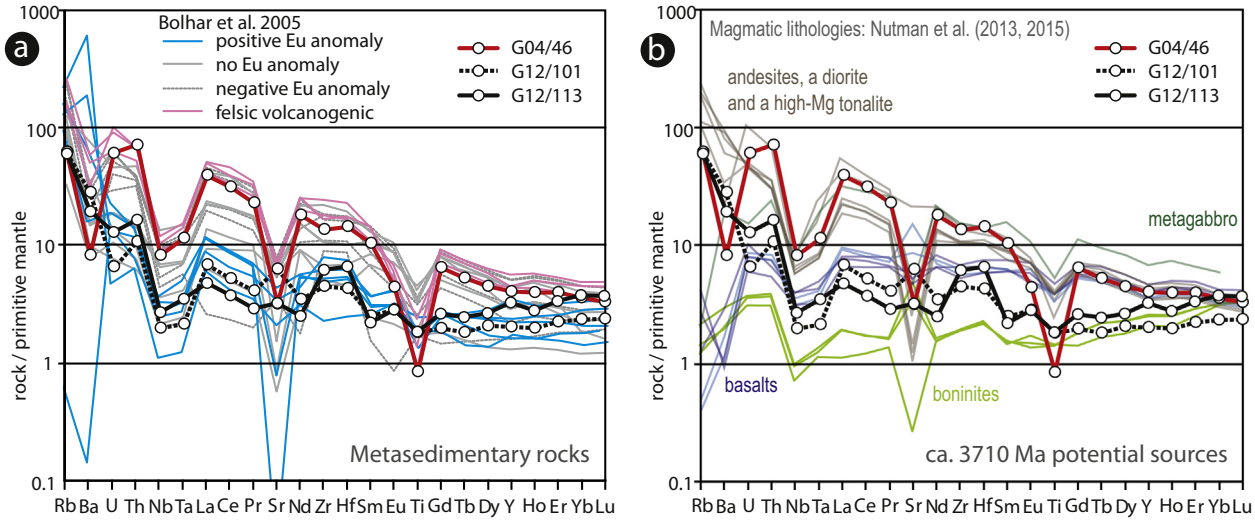

Fig. 4. Trace element patterns of investigated samples normalised to primitive mantle from Sun and McDonough (1989) compared to literature data. (a) Comparison with sedimentary lithologies from Isua (Bolhar et al., 2005). (b) Comparison with the ca. 3710 Ma magmatic lithologies (Nutman et al., 2013, 2015b).

This modification of the composition is in keeping with (i) the low yield of zircons in this sample (more akin with an andesitic rather than a dacitic or rhyolitic volcanic source) and (ii) the small size of the zircons (≤100 μm), suggesting rapid cooling of the source magma in an eruptive environment.

The zircon grains from this sample yield magmatic CL zoning and REE profiles, as well as mantle-like $\delta^{18}O$ (ca. +5.3‰). They yield a concordia age of 3709 ± 6 Ma, which is within the range of ages for volcanic rocks in the B2 unit (3700–3710 Ma, Kamber et al. 2005). The distinction between a strictly volcanic and a volcano-sedimentary origin cannot be made due to the lack of preserved structures. The euhedral shape of the zircon crystals, as well as trace element similarities between G04/46 and fresh andesites suggest that the protolith underwent no or limited sedimentary sorting and transport. This age is interpreted as the eruption age, or the source-rock age for this layer and it in turn constrains the deposition of the surrounding sediments to ca 3710 Ma at the earliest.

4.2. Weathering signatures within the 3700 Ma unit

The Itsaq Gneiss Complex rocks have been previously investigated for their oxygen isotope composition (Fig. 9). Oxygen isotopes have been measured in a variety of lithologies, either as whole rock (Baadsgaard et al., 1986; Cates and Mojzsis, 2006; Furnes et al., 2007; Pope et al., 2012) or mineral separates (Cates and Mojzsis, 2006; Pope et al., 2012), as well as in situ in zircon and olivine grains (Cates and Mojzsis, 2006; Hiess et al., 2009; Hiess et al., 2011).

The magmatic lithologies inferred to be the source for the B2

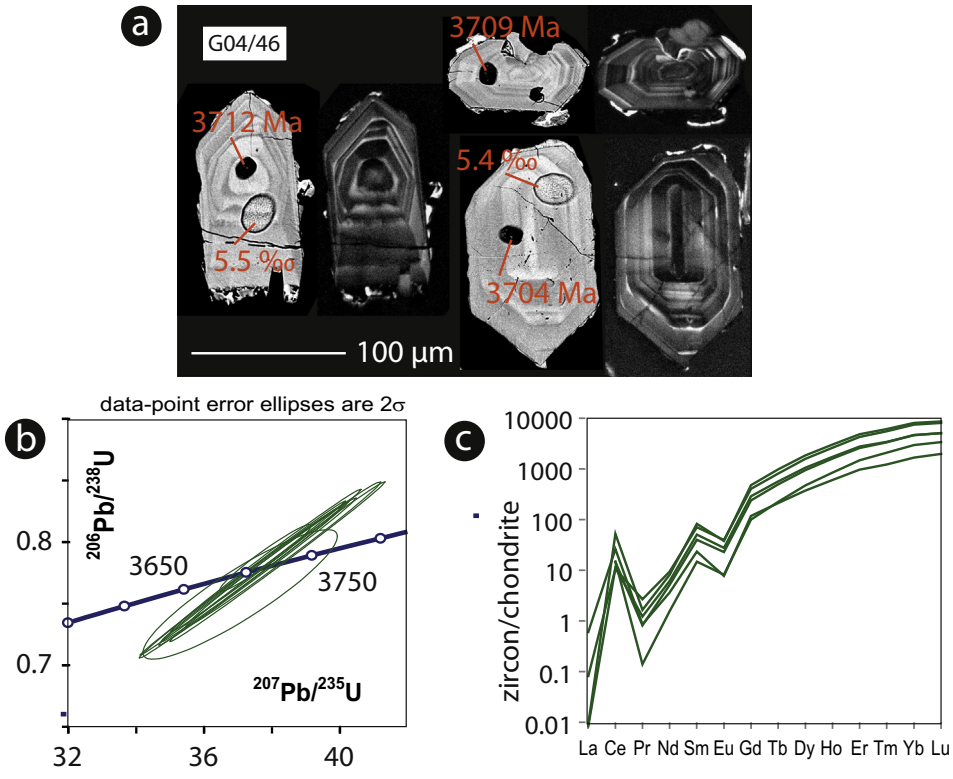

Fig. 5. (a) High-contrast BSE (left) and CL images (right) of selected zircon grains from felsic gneiss G04/46. The 204-corrected $^{206}Pb–^{207}Pb$ age (in Ma) is reported beside U–Pb dating pits (black). $\delta^{18}O$ values (in ‰) are reported beside the shallow SHRIMP pits. (b) Wetherill Concordia plot for 204-corrected U–Pb data. (c) REE composition of zircon normalised to CI chondrites of Sun and McDonough (1989) different shades of green are used for individual grains. (For interpretation of the references to colour in this figure legend, the reader is referred to the web version of this article.)

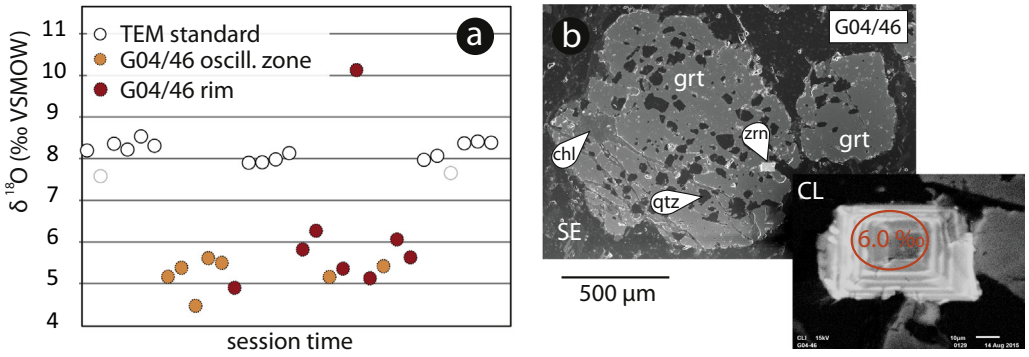

Fig. 6. (a) SHRIMP oxygen isotope analyses of Isua zircon plotted along session time (arbitrary scale). Internal 1SE bars are smaller than symbols. Shaded symbols are data points that were rejected on the basis of instrument parameters. (b) Secondary-electron image of G04/46 garnet with zircon inclusion; the cathodoluminescence images of the zircon is shown in the bottom right with marked the location of the oxygen isotope analysis and the $\delta^{18}O$ value.

sedimentary rocks (boninites, island-arc-tholeiites and andesites, Fig. 9), which outcrop in the 3700 Ma package of Isua supracrustal belt, yield mantle-like or slightly higher whole-rock $\delta^{18}O$ values. This signature is also recorded by magmatic zircon in G04/46 that yield mantle-like $\delta^{18}O$ values (+4.5 to +6‰). This can be recalculated (e.g. Valley et al., 2003) to a whole-rock value of +7 to +8‰ for the protolith magma, similar to the values reported for coeval quartz diorites and tonalities in the Isua supracrustal belt (Fig. 9). The $\delta^{18}O$ bulk rock values for sample G12/101, G12/113 and G04/46 (+11.6, +11.5 and +13.0 respectively, as reported in Nutman et al., 2017) are higher than reported values for any fresh, unaltered Isua 3700 Ma magmatic rocks. Low-temperature fluid-rock interaction is thus required to elevate the whole-rock $\delta^{18}O$ value to approximately +12‰ in the three samples studied here. The process of Eoarchean weathering has been documented in the Isua supracrustal belt: Nutman et al. (2017, 2019) reported whole-rock $\delta^{18}O$ values of between +15.7 to +16.8 for altered weathered mafic rocks located just below a ~3700 Ma unconformity in the *central tectonic domain*. They provide an analogue for the source-rock of the B2 schists. Other similar high $\delta^{18}O$ values are reported from a few other localities of the Itsaq Gneiss Complex, which is an indication that early, low temperature alteration/weathering might have been widespread. For example this is observed in an extensive felsic schist unit in the 3800 Ma package of the Isua supracrustal belt (Nutman et al., 2015b) as well as Akilia association biotite-quartz-garnet rocks ca. 200 km south of Isua (Cates and Mojzsis, 2006).

Temperatures required to enrich the $\delta^{18}O$ of silicates to this degree are below 200 °C (e.g. Sheppard et al., 1996 and references therein). The foremost mechanism by which high $\delta^{18}O$ are achieved on modern Earth is the formation of kaolinite, smectite and other clay minerals in weathering of magmatic/volcanic rocks exposed to the surface (e.g. Savin and Epstein, 1970). This surficial weathering process is supported by major element indicators as shown in Fig. 10 in the diagram of Ohata and Arai (2007) based on oxide proportions for Si, Ti, Al, Fe, Mg, Ca, Na and K. This diagram features a mafic-felsic trend where igneous rocks lie, the grey arrows represent weathering trends from the igneous poles as observed in soil weathering profiles. The major element composition of the mafic schists in the B2 unit forms a trend from the andesite field down to the weathering corner of the diagram corresponding to soils composition, in agreement with previous data on Isua metasedimentary rocks (Nutman et al., 2013; Bolhar et al., 2005). This trend represents leaching of low-temperature fluid-soluble elements, namely by replacement of plagioclases by kaolinite (or similar reactions forming clay minerals; Ohata and Arai, 2007).

4.3. Garnet growth in Isua B2 schists

Because of its large stability field and resistance to chemical re-equilibration, zoned garnet has the potential of recording multiple tectonic events, and with it variable $\delta^{18}O$ signatures. In order to unravel such complex evolution, a first step is identifying growth zones and their relationship to metamorphic/tectonic stages in the Isua supracrustal belt. In B2 samples G12/113 and G12/101, garnet is chemically zoned, as observed by previous authors in other samples from the same unit (Rollinson, 2002; Rollinson, 2003, and to a lesser extent Boak and Dymek, 1982). These garnet zones have sharp boundaries and are thought to relate to several stages of growth, and potentially metamorphic events.

The garnet core (Zone I, similar to Grt 1 in Rollinson, 2002) in samples G12/101 and G12/113 is Fe and Ca-poor. It yields decreasing Mn and HREE contents that are coherent with Rayleigh-fractionation during continuous growth. The marked negative Eu anomaly is indication for plagioclase presence during garnet growth. The core inclusions show a straight layering or foliation, which suggests no rotational deformation during its growth. As an indication, Boak and Dymek (1982) calculated garnet-biotite temperatures of 583 ± 30 and 542 ± 20 °C for garnet cores from two samples of schists with a similar assemblage and from the same unit of the investigated samples; however, this temperature was calculated using matrix biotite compositions that might have been reset during subsequent metamorphic events, moreover, the internal zoning of the garnet was not precisely documented. The growth of the garnet core is thus ascribed to prograde growth in a plagioclase bearing assemblage at amphibolite facies.

Two Ca-rich mantles (Zone II and III) surround the garnet core. These mantles have a sharp contact with the core. In G12/101, the Ca-rich mantles are depleted outwards in HREE and Mn. In G12/113, the HREE become depleted and then enriched, in an oscillatory pattern that resembles what is seen in Ca, and are likely due to concurring mineral reactions involving HREE-rich phases (Moore et al., 2013). Garnet zones of similar composition were reported by Rollinson (2003) as oscillatory zoned Garnet 2. Rollinson (2002) calculated temperatures of between 570 and 650 °C for early Garnet 2. The increased Ca in garnet is commonly interpreted as the sign of increased pressure (Rollinson, 2002; Rollinson, 2003). This record of increased pressure is in line with the presence of kyanite is some B2 samples (Boak and Dymek, 1982), for which a minimal pressure of 6 kbar was estimated. In G12/113 and other staurolite-bearing layers, the Ca-rich garnet rims seem texturally contemporaneous to staurolite porphyroblasts (now partially replaced by pseudomorphs) that deflect the main foliation. These Ca-rich mantles yield no Eu anomaly in both samples, which suggests that the co-existing assemblage was plagioclase-poor or absent. Absence of plagioclase is consistent with higher pressures, as plagioclase can react to form epidote-group minerals and amphibole at higher P conditions. The Ca-rich mantle is thus interpreted as grown in medium/high-P amphibolite conditions typical of Barrovian-type metamorphism associated with tectonic crustal thickening.

The outer Mg-rich and Ca-poor rim (Zone IV) of the garnet has a higher Mg# that corresponds to what reported by Rollinson (2003) for his Garnet 3. For this growth zone Rollinson (2002) calculated garnet-biotite T of ca. 530 °C (490–534 °C). Recalculated T from the data in Boak and Dymek (1982) yields. 487–516 °C and 480–509 °C for garnet rim and adjacent biotite pairs in two samples (using the same calibration of Perchuk and Lavrent'eva, 1983, for a range of P = 1 kbar to

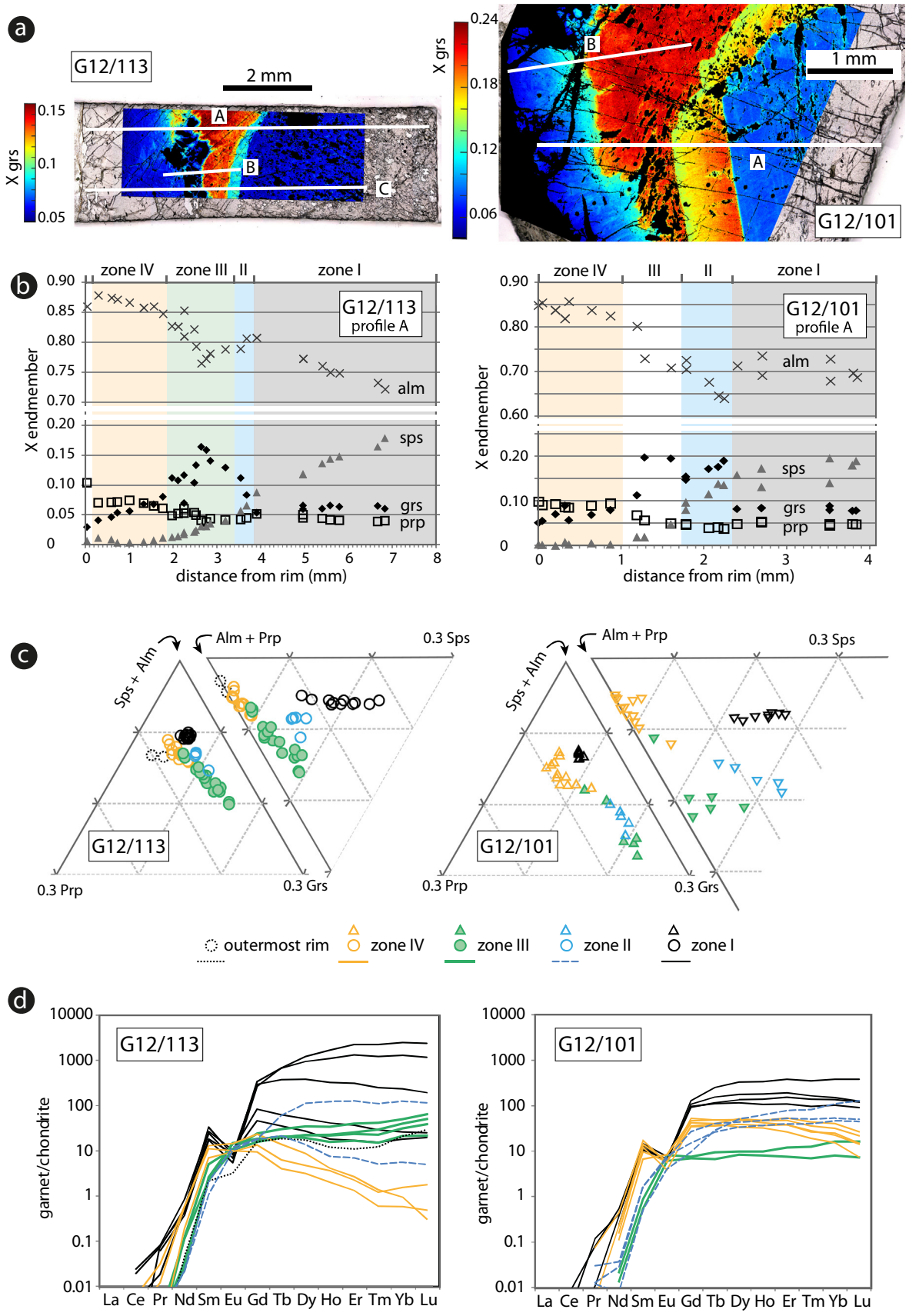

Fig. 7. Chemical composition of garnet from B2 schists. (a) EMPA garnet maps of XGrs superimposed on the transmitted light photograph of analysed garnet grains; the white lines indicate the location of the compositional profiles. (b) EDS endmember composition profiles according to distance to rim (analysis position projected on profile line, zones are distinguished on the basis of texture and chemistry). (c) Endmember composition of garnet zones. d. REE composition of different garnet zones normalised to CI chondrites of Sun and McDonough (1989).

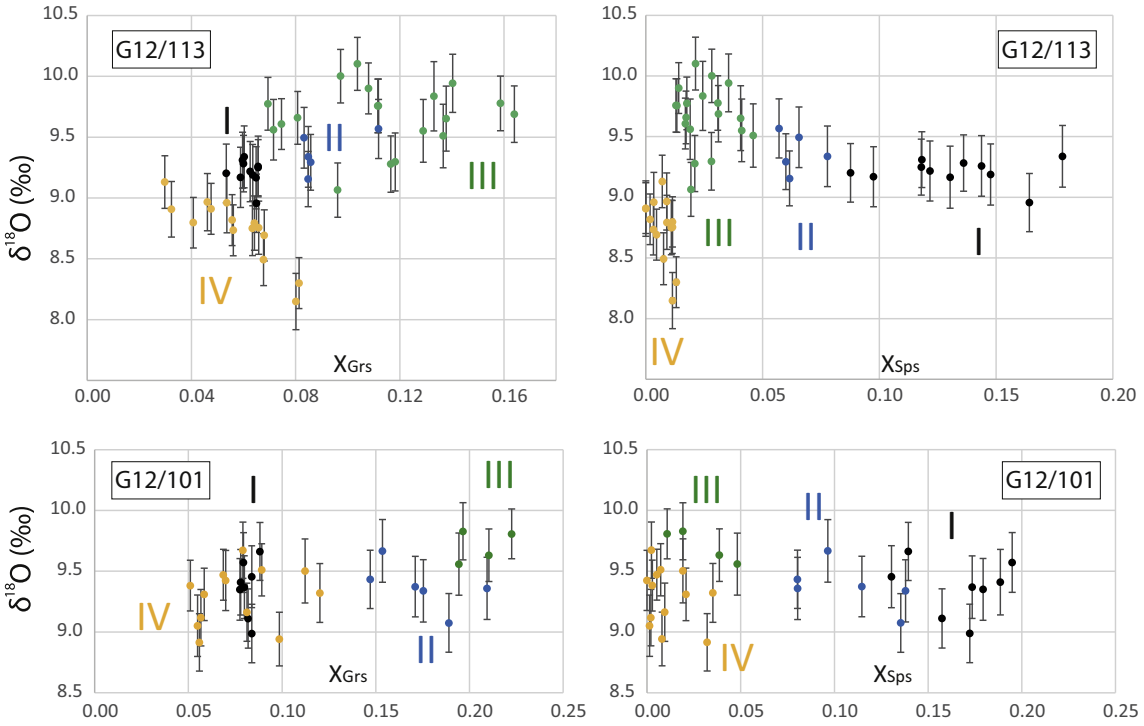

Fig. 8. SHRIMP IMF-corrected oxygen isotope analyses from profiles in G12/113 and G12/101 garnet, displayed according to their grossular and spessartine endmember content. Profile positions are indicated on Fig. 7. Figure $\delta^{18}O$ values are plotted with 1σ error bars. Symbol colour coding represents the garnet Zone I to IV as identified by texture and major elements in Fig. 7.

P = 6 kbar). In sample G12/101, the garnet rim yields a negative Eu anomaly, whereas garnet rim in G12/113 does not show a Eu anomaly. This difference reflects the bulk chemistry and in turn the matrix mineralogy: G12/101 yields 40 mode % of plagioclase and is relatively garnet poor, whereas sample G12/113 is poorer in Ca and Na and it contains abundant garnet, but only minor plagioclase. The garnet rim appears to grow statically on the previous foliation, and it is not present where quartz-filled pressure shadows are located. It grows over staurolite pseudomorphs in G12/113 and occasionally yields chloritoid inclusions that grow at the expanse of staurolite relicts, as seen in the matrix (Fig. 2b, Fig. 3a). The matrix minerals plagioclase and chloritoid and the absence of staurolite are indicative of upper greenschist to lower amphibolite facies, in line with previous estimates of 450–530 °C for garnet rim growth (Rollinson, 2002; Boak and Dymek, 1982).

4.4. Tectonic significance of garnet-growth zones

The garnet zoning is consistent with growth during different metamorphic stages at low and high-P geotherms. This evolution cannot be reconciled with prograde to retrograde evolution along a single P-T

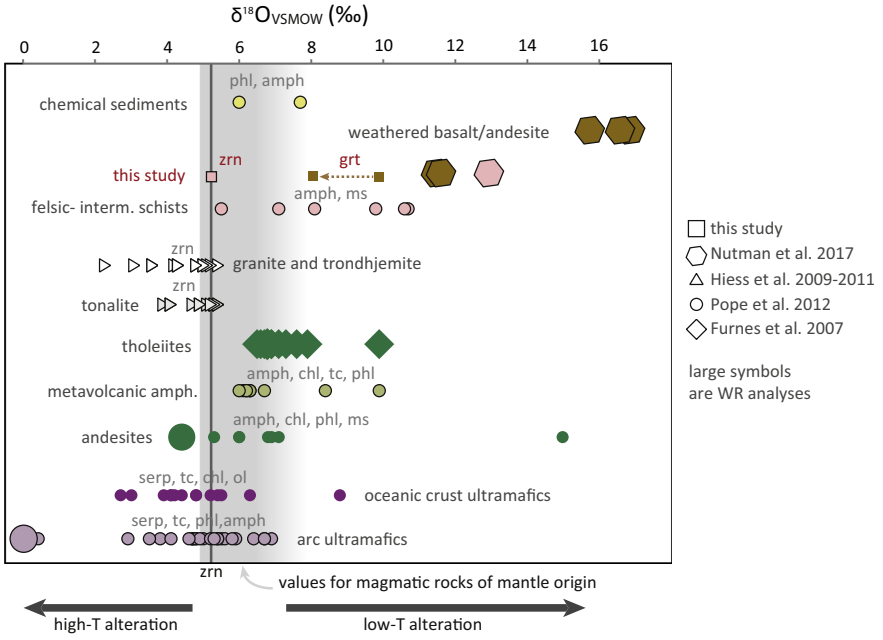

Fig. 9. Summary of oxygen isotope data for rocks of the 3700 Ma package of the Isua supracrustal belt, extracted from Hiess et al. (2009), Hiess et al. (2011), Pope et al. (2012), Furnes et al. (2007) and Baadsgaard et al. (1986) according to the geochronology and mapping of Nutman and Friend (2009). Mantle zircon value is taken from Valley et al. (1998), the grey band represents the range of magmatic rocks derived from the mantle, following fractional crystallization with little alteration. Square symbols represent minerals data acquired from the samples studied in this work; corresponding whole-rock analyses were reported in Nutman et al. (2017) as part of a larger dataset.

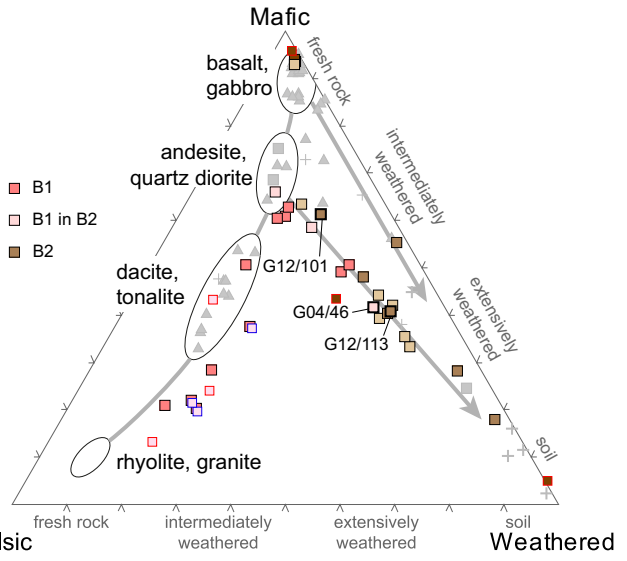

Fig. 10. Weathering diagram of Ohata & Arai (2007) for samples G12/101, G12/113 and G04/46 together with B1 felsic schists and B2 mafic schists (pink and brown squares, respectively), with representative ~3700 Ma lithologies (grey symbols, Nutman et al.,2015b). B1 and B2 literature data is from Nutman et al. (2013) in the black outlines, Bolhar et al. (2005) in the blue outlines. (For interpretation of the references to colour in this figure legend, the reader is referred to the web version of this article.)

path (e.g. Komiya et al., 2002), but requires overprinting tectono-metamorphic events.

The chemistry of B2 schists garnet cores is specific to the tectonic slice containing the B2 unit, and has not been detected in garnet anywhere else in the Isua supracrustal belt (Rollinson, 2002). The growth of the cores thus indicates a first prograde metamorphism before the assembly of the 3700 Ma package subdomains. A plausible tectonic setting for the formation of the garnet cores would be high heat-flow metamorphism, shortly after deposition of the B2 mafic schists in the environment described by Nutman et al. (2015b).

The temperature for garnet core and mantle growth (with the presence of staurolite) is higher than what is recorded in the metamorphosed Ameralik dykes that crosscut the Isua supracrustal belt (intruded at 3500 Ma, maximal temperature of metamorphic equilibration of around 550 °C, Rollinson, 2002). This higher recorded temperature demonstrates that garnet Zones I to III grew during Eoarchaean, before 3500 Ma. This mid–high P metamorphism and deformation can be correlated to a crustal thickening event during the 3690–3660 assembly of the 3700 and the 3800 Ma packages: the Itsukasian orogeny described by Nutman et al. (2015b). Crust-stacking was followed by extensional high-heat flow pan-Itsaq Gneiss Complex metamorphism at ca. 3600 Ma (Nutman et al., 2014; Nutman et al., 2015c). In absence of direct dating of the garnet, the chronology of the crust-stacking and extensional events has been established on the basis of (i) cross-cutting relationships (see summary in Nutman and Friend, 2009), (ii) rare relicts of high-pressure granulites with an age of 3660 Ma, present within the gneisses north of the Isua supracrustal belt (Nutman et al., 2014; Nutman et al., 2015c) (iii) titanite and zircon ages of 3630–3620 Ma for amphibolite-facies metamorphism (Crowley and Myers, 2002; Crowley, 2003).

The lower grade conditions recorded in the garnet outer rim corresponds to conditions observed widely in the Isua Supracrustal Belt (Garnet 3 in most tectonic zones of Rollinson, 2002), including the upper greenschist-lower amphibolite metamorphic facies overprinting the Ameralik dykes (Nutman, 1986; Rollinson, 2002). The outer garnet rim in the B2 schists records a lower temperature than recorded by the inner zones of the garnet (garnet-biotite temperature of 650 °C in Rollinson, 2002, and presence of staurolite). Formation of garnet on the retrograde path is not expected in Barrovian metamorphism of metapelites. It is thus likely that this zone formed during a separate tectonic event whose peak temperature was lower. This inference is supported by the textural evidence that the garnet rim grew statically over a pre-existing higher T foliation, and over staurolite pseudomorphs after staurolite retrogression. We speculate that the garnet rim corresponds to the late Archaean metamorphic event in the uppermost greenschist facies to lower amphibolite facies experienced by the Itsaq complex. In Isua, the most significant post Ameralik dyke metamorphism occurred at ca. 2690 Ma (e.g. Nutman et al., 2015b and references therein).

4.5. Tracking WR $\delta^{18}O$ through geologic time

Garnet $\delta^{18}O$ values allow tracking back the whole-rock signature through geologic time. It has been shown that diffusivity of oxygen in garnet during metamorphism is negligible to T of at least 600 °C (Page et al., 2014; Rubatto and Angiboust, 2015) and it oxygen isotopic signature may be retained up to 800 °C (e.g. Vielzeuf et al., 2005; Higashino et al., 2019). G12/101 and G12/113 schists contain metamorphic garnet with $\delta^{18}O$ values of +8.7 to +9.7‰ that are significantly higher than the $\delta^{18}O$ values of +5.4 ± 0.4‰ for magmatic zircon in felsic rock G04/46 (oxygen isotope fractionation between zircon and almandine garnet at T > 500 °C is < 0.12‰, based on fractionation factors of Valley et al., 2003). All garnet zones, in both mafic samples (and the few indicative analyses in G04/46) yield similar high $\delta^{18}O$ values (9.5 ± 1‰). The single zircon rim measured at 10.1‰ in G04/46 could speculatively represent minor metamorphic zircon dissolution-reprecipitation, in equilibrium with the garnet bearing assemblage.

Calculations confirm that that the measured bulk rock $\delta^{18}O$ value is in equilibrium with the measured garnet oxygen composition, and it has not been affected by post-metamorphic alteration. A simple model was calculated (Supplementary material 8) at temperatures of 500, 550 and 610 °C(Boak and Dymek, 1982; Rollinson, 2002), the modal composition for the 5 major minerals in each sample and oxygen fractionation factors from Zheng (1993a, 1993b). For G12-101, the modelled $\delta^{18}O$ WR-values in equilibrium with the four garnet zones vary between ca. +11.2 and +11.5‰, in agreement with the measured bulk rock value of +11.6‰ (reported in Nutman et al., 2017). For G12-113, the modelled $\delta^{18}O$ values vary from ca. +11.2 to +11.7‰, again matching the measured bulk rock value of 11.5‰ (reported in Nutman et al., 2017). This agreement demonstrates that sample G12-101 and G12-113 remained a closed system for oxygen isotopes since the growth of the first garnet zone. The minor $\delta^{18}O$ decrease between measured values of garnet zone III and IV (−0.4‰ in G12-101 and −0.7‰ in G12-113) is at the limit of our analytic precision. The calculated model shows that a $\delta^{18}O$ decrease of this magnitude in garnet is expected for a minor decrease in temperature in a closed system (from > 600 °C down to 500 °C), and does not require the input of external fluids. The result is similar to the model of Kohn et al. (1993) that predicts a variation in garnet $\delta^{18}O$ of ca. 1‰ over 100 °C for metapelites.

The results implies that the Isua B2 metasedimentary rocks had acquired their high $\delta^{18}O$ values at the surface, and transported this $\delta^{18}O$ signature in the Archean crust before early mid temperature metamorphism at ca. 3660–3690 Ma (age attributed to the garnet cores, see above), and certainly before 3500 Ma (age of lower grade cross-cutting Ameralik dykes) (Fig. 11). Metamorphism of these sediments followed within 10 to 50 My of sedimentation, which demonstrates the possibility for early and fast recycling of surficial oxygen isotope signatures in the early Archean crust. The same process is recorded in the Archaean high-grade metasedimentary rocks of the Pilbara, Australia (François et al., 2014) and in the felsic meta-igneous crust of the Saglek Block in the North Atlantic Craton (Vezinet et al., 2019). In contrast to previously identified high $\delta^{18}O$ Eoarchean lithologies such as refractory BIFs and dolomites or low-volume altered horizons (3800 Ma Isua

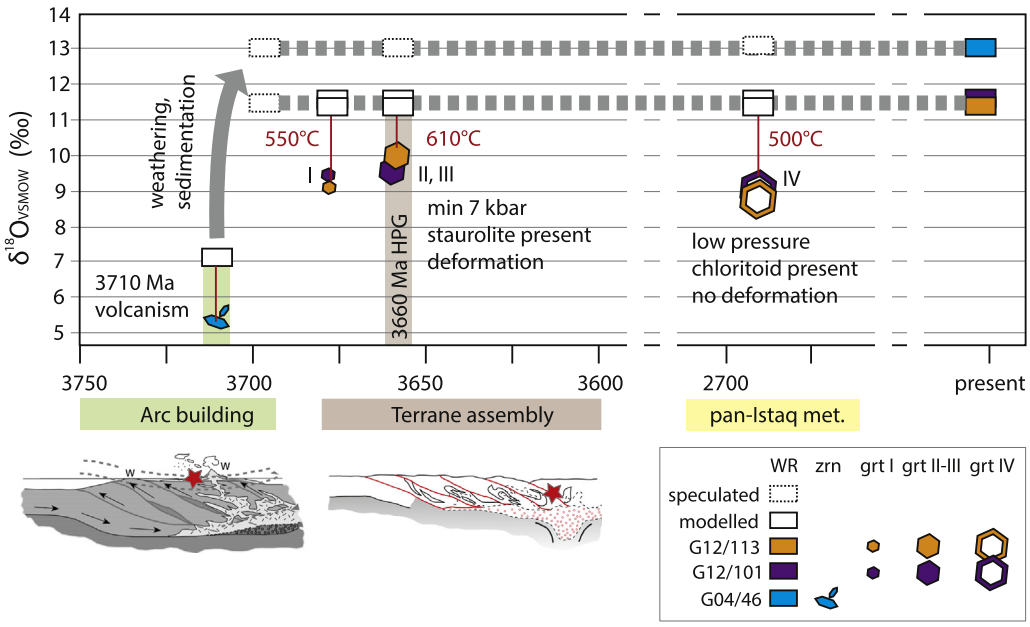

Fig. 11. Summary of $\delta^{18}O$ data for B2 schists on the timeline of tectonic events in the Isua Supracrustal Belt. Measured zircon and garnet values are represented by filled symbols. Red lines show equilibrium relationships between measured minerals and modelled bulk rock at the temperatures shown in red. Sketch for arc building is taken from Nutman et al. (2013), and for terrane assembly including formation of a high-pressure granulite (HPG) from Nutman et al. (2015c). Red stars indicate the position of B2 schists at the different stages. (For interpretation of the references to colour in this figure legend, the reader is referred to the web version of this article.)

package weathered volcanics, Nutman et al., 2015a) and thin sedimentary layers (e.g. Akilia association metasedimentary rocks, Cates and Mojzsis, 2006), these rocks provide a volumetrically important fertile source for high $\delta^{18}O$ crustal magmas (undiluted +12‰). Melting of these sedimentary rocks can explain high $\delta^{18}O$ zircon grains as the result of S-type granite formation early in Earth's history (e.g., Mojzsis et al., 2001; Peck et al., 2001; Trail et al., 2007).

Many tectonic models that have been proposed for the Isua belt on the basis of structural and petrographic studies are akin to modern subduction (e.g., Komiya et al., 1999; Hayashi et al., 2000; Arai et al., 2014) or flat subduction (Friend and Nutman, 2005; Nutman et al., 2014; Nutman et al., 2015c; Kaczmarek et al., 2016) followed by collisional orogeny. The latter subduction model is in agreement with the observations here, and where relatively fast burial to mid- to lower-crustal depth is facilitated during orogeny, as slivers of arc crust are juxtaposed and stacked.

5. Conclusions

1) 3700 Ma volcano-sedimentary rocks of the Isua supracrustal represent surficial lithologies with an elevated $\delta^{18}O$. Their elevated $\delta^{18}O$ value was acquired on the surface from low-temperature alteration such as weathering of mantle-derived 3700–3710 Ma arc rocks.
2) The alteration is marked by the offset between $\delta^{18}O$ values in 3709 Ma zircon that record the magmatic signature (ca. +5.3‰) and the whole rock $\delta^{18}O$ values (ca. +12‰).
3) The low temperature whole rock signature is inherited by garnet with $\delta^{18}O$ values of +8.7 to +9.7‰ and that records several phases of Archean metamorphism, including the crustal stacking event that buried these lithologies to amphibolite facies conditions estimated to have occurred at 3660 to 3650 Ma.
4) The combined $\delta^{18}O$ values of the metasedimentary whole rocks and the zircon and garnet they contain require that the mafic protoliths crystallised from a mantle source, experienced low temperature alteration/weathering to acquire elevated $\delta^{18}O$, and were buried to mid-crustal levels forming high $\delta^{18}O$ garnet in a short period of time- within 10–50 My.
5) Such crustal recycling occurring where temperatures reached partial melting, could have produced Eoarchaean and potentially Hadean high $\delta^{18}O$ magmatic zircon within tens of millions of years after the formation of the surficial lithologies.

Declaration of competing interest

The authors declare that they have no known competing financial interests or personal relationships that could have appeared to influence the work reported in this paper.

Acknowledgements

Jörg Hermann, Jade-Star Lackey, Axel Schmitt, an anonymous reviewer and three anonymous thesis examiners are thanked for constructive comments. Pierre Lanari kindly assisted the production of EPMA maps. This work was funded by Australian Research Council projects DP120100273 and DP170100715. DR acknowledges the support of ARC grant DP110101599 and Swiss National Science Foundation grant 200021-166280.

Appendix A. Supplementary data

Supplementary data to this article can be found online at https://doi.org/10.1016/j.chemgeo.2020.119474.

References

Appel, P.W.U., Fedo, C.M., Moorbath, S., Myers, J., 1998. Recognizable primary volcanic and sedimentary features in a low-strain domain of the highly deformed, oldest known (~ 3.7-3.8 Gyr) Greenstone Belt, Isua, West Greenland. Terra Nov 10, 57–62. https://doi.org/10.1046/j.1365-3121.1998.00162.x.

Ávila, J.N., Ireland, T.R., Holden, P., Lanc, P., Latimore, A., Schram, N., Foster, J., Williams, I.S., Loiselle, L., Fu, B., 2020. High-Precision, High-Accuracy Oxygen Isotope Measurements of Zircon Reference Materials with the SHRIMP-SI. Geostand Geoanal Res. https://doi.org/10.1111/ggr.12298.

Arai, T., Omori, S., Komiya, T., Maruyama, S., 2014. Intermediate P/T-type regional metamorphism of the Isua Supracrustal Belt, southern west Greenland: the oldest Pacific-type orogenic belt? Tectonophysics 662, 22–39. https://doi.org/10.1016/j.tecto.2015.05.020.

Baadsgaard, H., Nutman, A.P., Rosing, M.T., et al., 1986. Alteration and metamorphism of Amitsoq gneisses from the Isukasia area, West Greenland: Recommendations for isotope studies of the early crust. Geochim. Cosmochim. Acta 50, 2165–2172. https://doi.org/10.1016/0016-7037(86)90071-2.

Black, L.P., et al., 2004. Improved 206 Pb/238 U microprobe geochronology by the monitoring of a trace element-related matrix effect; SHRIMP, ID–TIMS, ELA–ICP–MS and oxygen isotope documentation for a series of zircon standards. Chem Geol 205, 115–140.

Blichert-Toft, J., Frei, R., 2001. Complex Sm-Nd and Lu-Hf isotope systematics in

metamorphic garnets from the Isua supracrustal belt, West Greenland. Geochim. Cosmochim. Acta 65, 3177–3189. https://doi.org/10.1016/S0016-7037(01)00680-9.
Boak, J., Dymek, R.F., 1982. Metamorphism of the ca. 3800 Ma supracrustal rocks at Isua, West Greenland: implications for early Archaean crustal evolution. Earth Planet. Sci. Lett. 59, 155–176. https://doi.org/10.1016/0012-821X(82)90123-6.
Bolhar, R., Kamber, B.S., Moorbath, S., et al., 2004. Characterisation of early Archaean chemical sediments by trace element signatures. Earth Planet. Sci. Lett. 222, 43–60. https://doi.org/10.1016/j.epsl.2004.02.016.
Bolhar, R., Kamber, B.S., Moorbath, S., et al., 2005. Chemical characterization of earth's most ancient clastic metasediments from the Isua Greenstone Belt, southern West Greenland. Cosmochim Acta 69, 1555–1573.
Cates, N.L., Mojzsis, S.J., 2006. Chemical and isotopic evidence for widespread Eoarchean metasedimentary enclaves in southern West Greenland. Geochim. Cosmochim. Acta 70, 4229–4257. https://doi.org/10.1016/j.gca.2006.05.014.
Crowley, J.L., 2003. U-Pb geochronology of 3810-3630 Ma granitoid rocks south of the Isua greenstone belt, southern West Greenland. Precambrian Res. 126, 235–257. https://doi.org/10.1016/s0301-9268(03)00097-4.
Crowley, J.L., Myers, J., 2002. Timing and Nature of Multiple 3700–3600 Ma Tectonic Events in Intrusive Rocks North of the Isua Greenstone Belt, Southern West Greenland.
Dymek, R.F., Boak, J., Gromet, L., 1983. Average Sedimentary Rock Rare Earth Element Patterns and Crustal Evolution: Some Observations and Implications From the 3800 Ma ISUA Supracrustal Belt, West Greenland.
François, C., Philippot, P., Rey, P.F., Rubatto, D., 2014. Burial and exhumation during Archean sagduction in the East Pilbara Granite-Greenstone Terrane. Earth Planet. Sci. Lett. 396, 235–251. https://doi.org/10.1016/j.epsl.2014.04.025.
Friend, C.R.L., Nutman, A.P., 2005. Complex 3670–3500 Ma Orogenic Episodes Superimposed on Juvenile Crust Accreted between 3850 and 3690 Ma. Itsaq Gneiss Complex, southern West Greenland.
Furnes, H., de Wit, M., Staudigel, H., et al., 2007. A vestige of Earth's oldest ophiolite. Science (80-) 315, 1704–1707. https://doi.org/10.1126/science.1139170.
Gregory, R.T., Taylor, H.P., 1981. An oxygen isotope profile in a section of Cretaceous oceanic crust, Samail Ophiolite, Oman: evidence for δ18O buffering of the oceans by deep (> 5 km) seawater-hydrothermal circulation at mid-ocean ridges. J. Geophys. Res. Solid Earth 86, 2737–2755. https://doi.org/10.1029/JB086iB04p02737.
Hayashi, M., Komiya, T., Nakamura, Y., Maruyama, S., 2000. Archean Regional Metamorphism of the Isua Supracrustal Belt, Southern West Greenland: Implications for a Driving Force for Archean Plate Tectonics. Int. Geol. Rev. 42, 1055–1115. https://doi.org/10.1080/00206810009465128.
Hiess, J., Bennett, V.C., Nutman, A.P., Williams, I.S., 2009. In situ U–Pb, O and Hf isotopic compositions of zircon and olivine from Eoarchaean rocks, West Greenland: New insights to making old crust. Geochim. Cosmochim. Acta 73, 4489–4516.
Hiess, J., Bennett, V.C., Nutman, A.P., Williams, I.S., 2011. Archaean fluid-assisted crustal cannibalism recorded by low δ18O and negative εHf(T) isotopic signatures of West Greenland granite zircon. Contrib to Mineral Petrol 161, 1027–1050. https://doi.org/10.1007/s00410-010-0578-z.
Higashino, F., Rubatto, D., Kawakami, T., Bouvier, A.-S., Baumgartner, L.P., 2019. Oxygen isotope speedometry in granulite facies garnet recording fluid/melt–rock interaction (Sør Rondane Mountains, East Antarctica). J. Metamorph. Geol. 37, 1037–1048.
Hoskin, P.W.O., Schaltegger, U., 2003. The composition of zircon and igneous and metamorphic petrogenesis. Rev Mineral geochemistry 53, 27–62.
Ickert, R.B., et al., 2008. Determining high precision, in situ, oxygen isotope ratios with a SHRIMP II: analyses of MPI-DING silicate-glass reference materials and zircon from contrasting granites. Chem Geol 257, 114–128. https://doi.org/10.1016/j.chemgeo.2008.08.024.
Kaczmarek, M.-A., Reddy, S.M., Nutman, A.P., et al., 2016. Earth's oldest mantle fabrics indicate Eoarchaean subduction. Nat. Commun. 7, 10665. https://doi.org/10.1038/ncomms10665.
Kamber, B.S., Whitehouse, M.J., Bolhar, R., 2005. Volcanic resurfacing and the early terrestrial crust: zircon U–Pb and REE constraints from the Isua Greenstone Belt, southern West Greenland. Earth Planet 240, 276–290.
Kohn, M.J., Valley, J.W., Elsenheimer, D., Spicuzza, M.J., 1993. O isotope zoning in garnet and staurolite: evidence for closed- system mineral growth during regional metamorphism. Am. Mineral. 78, 988–1001.
Komiya, T., Maruyama, S., Masuda, T., et al., 1999. Plate tectonics at 3.8-3.7 Ga: field evidence from the Isua accretionary complex, southern West Greenland. J 107, 515–554. https://doi.org/10.1086/314371.
Komiya, T., Hayashi, M., Maruyama, S., Yurimoto, H., 2002. Intermediate-P/T type Archean metamorphism of the Isua supracrustal belt: Implications for secular change of geothermal gradients at subduction zones and for Archean plate tectonics. Am. J. Sci. 302, 806–826. https://doi.org/10.2475/ajs.302.9.806.
Lanari, P., Guillot, S., Schwartz, S., et al., 2012. Diachronous evolution of the alpine continental subduction wedge: evidence from P-T estimates in the Briançonnais Zone houillère (France - Western Alps). J. Geodyn. 56–57, 39–54. https://doi.org/10.1016/j.jog.2011.09.006.
Lanari, P., Riel, N., Guillot, S., et al., 2013. Deciphering high-pressure metamorphism in collisional context using microprobe mapping methods: Application to the Stak eclogitic massif (northwest Himalaya). Geology 41, 111–114. https://doi.org/10.1130/G33523.1.
Lanari, P., Burn, M., Loury, C., et al., 2014. XMapTools a program for X-ray images processing and thermobarometric studies. Geophys. Res. Abstr. https://doi.org/10.1103/PhysRevB.82.161108.
Lawrence, J., Taylor, H.P., 1971. Deuterium and Oxygen-18 Correlation: Clay Minerals and Hydroxides in Quaternary Soils Compared to Meteoric Waters.
Ludwig, K., 2009. SQUID 2 (Rev. 2.50): A User's Manual Berkeley Geochronology Center Spec Pub 5. (104p).
Ludwig, K.R., 2012. User's Manual for Isoplot 3.75. A Geochronological Toolkit for Microsoft Excel. Berkeley Geochronol Center Spec Pub 5 (75p).
Martin, L.A.J., Rubatto, D., Crépisson, C., et al., 2014. Garnet oxygen analysis by SHRIMP-SI: Matrix corrections and application to high-pressure metasomatic rocks from Alpine Corsica. Chem. Geol. 374–375, 25–36. https://doi.org/10.1016/j.chemgeo.2014.02.010.
McGregor, V.R., 1973. The early Precambrian gneisses of the Godthåb district, West Greenland. Philos. Trans. R. Soc. Lond. A273, 343–358.
Mojzsis, S.J., Harrison, T.M., Pidgeon, R.T., 2001. Oxygen-isotope evidence from ancient zircons for liquid water at the Earth's surface 4,300 Myr ago. Nature 409, 178–181. https://doi.org/10.1038/35051557.
Moore, S.J., Carlson, W.D., Hesse, M.A., 2013. Origins of yttrium and rare earth element distributions in metamorphic garnet. J Metamorphic Geol 31 (6), 663–689. https://doi.org/10.1111/jmg.12039.
Nutman, A.P., 1986. The early Archaean to Proterozoic history of the Isukasia area, Southern West Greenland. In: Bulletin of the Geological Survey of Greenland. 154 (80pp).
Nutman, A.P., Bridgwater, D., 1986. Early Archaean Amitsoq Tonalites and Granites of the Isukasia Area, Southern West Greenland: Development of the Oldest-Known Sial.
Nutman, A.P., Collerson, K.D., 1991. Very early Archean crustal-accretion complexes preserved in the North Atlantic Craton. Geology 19, 791–795.
Nutman, A.P., Friend, C.R.L., 2009. New 1:20,000 scale geological maps, synthesis and history of investigation of the Isua supracrustal belt and adjacent orthogneisses, southern West Greenland: a glimpse of Eoarchaean crust formation and orogeny. Precambrian Res. 172, 189–211.
Nutman, A.P., Allaart, J.H., Bridgwater, D., et al., 1984. Stratigraphic and geochemical evidence for the depositional environment of the early Archaean Isua Supracrustal Belt, southern west Greenland. Precambrian Res. 25, 365–396. https://doi.org/10.1016/0301-9268(84)90010-X.
Nutman, A.P., Hagiya, H., Maruyama, S., 1995. SHRIMP U-Pb single zircon geochronology of a Proterozoic mafic dyke, Isukasia, southern West Greenland. Bull. Geol. Soc. 42, 16–20 Denmark.
Nutman, A.P., Bennett, V.C., Friend, C.R.L., Rosing, M.T., 1997. ~ 3710 and ⩾ 3790 Ma volcanic sequences in the Isua (Greenland) supracrustal belt; structural and Nd isotope implications. Chem. Geol. 141, 271–287. https://doi.org/10.1016/S0009-2541(97)00084-3.
Nutman, A.P., Bennett, V.C., Friend, C.R.L., McGregor, V.R., 2000. The early Archaean Itsaq Gneiss Complex of Southern West Greenland: the importance of field observations in interpreting age and isotopic constraints for early terrestrial evolution. Geochimica Cosmochimica Acta 64, 3035–3060.
Nutman, A.P., Friend, C.R.L., Bennett, V.C., 2004. Dating of the Ameralik dyke swarms of the Nuuk district, southern West Greenland: Mafic intrusion events starting from c. 3510 Ma. J. Geol. Soc. Lond. 161, 421–430.
Nutman, A.P., Bennett, V.C., Friend, C.R.L., Hidaka, H., Yi, K., Lee, S.R., Kamiichi, T., 2013. Episodic 3920-3660 Ma juvenile crust formation and 3660-3600 Ma recycling in the Itsaq Gneiss Complex of southern West Greenland. Am. J. Sci. 313, 877–911. https://doi.org/10.2475/09.2013.00.
Nutman, A.P., Bennett, V.C., Friend, C.R.L., et al., 2014. The itsaq gneiss complex of Greenland: Episodic 3900 to 3660 Ma juvenile crust formation and recycling in the 3660 to 3600 Ma Isukasian orogeny. Am. J. Sci. https://doi.org/10.2475/09.2013.03.
Nutman, A.P., Bennett, V.C., Chivas, A.R., et al., 2015a. 3806Ma Isua rhyolites and dacites affected by low temperature Eoarchaean surficial alteration: Earth's earliest weathering. Precambrian Res. 268, 323–338. https://doi.org/10.1016/j.precamres.2015.07.014.
Nutman, A.P., Bennett, V.C., Friend, C.R.L., 2015b. The Emergence of the Eoarchaean Proto-Arc: Evolution of a c. 3700 Ma Convergent Plate Boundary at Isua, Southern West Greenland.
Nutman, A.P., Bennett, V.C., Friend, C.R.L., 2015c. Proposal for a continent "Itsaqia" amalgamated at 3.66 Ga and rifted apart from 3.53 Ga: Initiation of a Wilson cycle near the start of the rock record. Am. J. Sci. 315, 509–536. https://doi.org/10.2475/06.2015.01.
Nutman, A.P., Bennett, V.C., Friend, C.R.L., Chivas, A.R., 2017. The Isua Supracrustal Belt of the North Atlantic Craton (Greenland). In: Sediment Provenance. Elsevier, pp. 563–592.
Nutman, A.P., Bennett, V.C., Friend, C.R.L., Van Kranendonk, M., Chivas, A.R., 2019. Reconstruction of a 3700 Ma transgressive marine environment from Isua (Greenland): Sedimentology, stratigraphy and geochemical signatures. Lithos. https://doi.org/10.1016/j.lithos.2019.105164.
Ohata, T., Arai, H., 2007. Statistical empirical index to chemical weathering in igneous rocks: A new tool for evaluating the degree of weathering. Chemical Geology 240, 280–297.
Page, F.Z., Essene, E.J., Mukasa, S.B., Valley, J.W., 2014. A garnet-zircon oxygen isotope record of subduction and exhumation fluids from the Franciscan complex. California. J Petrol 55, 103–131. https://doi.org/10.1093/petrology/egt062.
Paton, C., Hellstrom, J., Paul, B., et al., 2011. Iolite: Freeware for the visualisation and processing of mass spectrometric data. J. Anal. At. Spectrom. 26, 2508–2518. https://doi.org/10.1039/c1ja10172b.
Peck, W.H., Valley, J.W., Wilde, S.A., Graham, C.M., 2001. Oxygen isotope ratios and rare earth elements in 3.3 to 4.4 Ga zircons: Ion microprobe evidence for high δ18O continental crust and oceans in the early Archean. Geochim. Cosmochim. Acta 65, 4215–4229. https://doi.org/10.1016/S0016-7037(01)00711-6.
Perchuk, L.L., Lavrent'eva, I.V., 1983. Experimental Investigation of Exchange Equilibria in the System Cordierite-Garnet-Biotite. Springer, New York, pp. 199–239.

Polat, A., Hofmann, A., Rosing, M.T., 2002. Boninite-like volcanic rocks in the 3.7–3.8 Ga Isua greenstone belt, West Greenland: geochemical evidence for intra-oceanic subduction zone processes in the early. Chem. Geol. 184, 231–254. https://doi.org/10.1016/S0009-2541(01)00363-1.

Pope, E.C.E., Bird, D.K., Rosing, M.T., 2012. Isotope composition and volume of Earth's early oceans. Proc. Natl. Acad. Sci. U. S. A. 109, 4371–4376. https://doi.org/10.1073/pnas.1115705109.

Rollinson, H., 2002. The metamorphic history of the Isua Greenstone Belt, West Greenland. Geol Soc London, Spec Publ 199, 329–350. https://doi.org/10.1144/GSL.SP.2002.199.01.16.

Rollinson, H., 2003. Metamorphic history suggested by garnet-growth chronologies in the Isua Greenstone Belt, West Greenland. Precambrian Res. 181–196.

Rosing, M.T., 1999. 13C-depleted carbon microparticles in > 3700-Ma Sea-floor sedimentary rocks from west Greenland. Science (80-) 283, 674–676. https://doi.org/10.1126/science.283.5402.674.

Rubatto, D., Angiboust, S., 2015. Oxygen isotope record of oceanic and high-pressure metasomatism: a P–T–time–fluid path for the Monviso eclogites (Italy). Contrib to Mineral Petrol 170, 44. https://doi.org/10.1007/s00410-015-1198-4.

Savin, S.M., Epstein, S., 1970. The oyxgen and hydrogen isotope geochemistry of ocean sediments and shales. Geochim. Cosmochim. Acta 34, 43–63. https://doi.org/10.1016/0016-7037(70)90150-X.

Sheppard, S., Gilg, H., Sheppard, S.M.F., Gilg, H.A., 1996. Stable isotope geochemistry of clay minerals. Clay Miner. 31, 1–24.

Spandler, C.J., Pettke, T., Rubatto, D., 2011. Internal and external fluid sources for eclogite-facies veins in the Monviso Meta-ophiolite, Western Alps: Implications for fluid flow in subduction zones. J Petrol 52, 1207–1236. https://doi.org/10.1093/petrology/egr025.

Stacey, J.S.T., Kramers, J., 1975. Approximation of terrestrial lead isotope evolution by a two-stage model. Earth Planet. Sci. Lett. 26, 207–221.

Sun, S.-S., McDonough, W.F., 1989. Chemical and isotopic systematics of oceanic basalts: implications for mantle composition and processes. Geol Soc London, Spec Publ 42, 313–345.

Trail, D., Mojzsis, S.J., Harrison, T.M., et al., 2007. Constraints on Hadean zircon protoliths from oxygen isotopes, Ti-thermometry, and rare earth elements. Geochemistry, Geophys Geosystems. https://doi.org/10.1029/2006GC001449.

Valley, J.W., Kitchen, N., Kohn, M.J., et al., 1995. UWG-2, a garnet standard for oxygen isotope ratios: strategies for high precision and accuracy with laser heating. Geochim. Cosmochim. Acta 59, 5223–5231. https://doi.org/10.1016/0016-7037(95)00386-X.

Valley, J.W., Kinny, P.D., Schulze, D.J., Spicuzza, M.J., 1998. Zircon megacrysts from kimberlite: oxygen isotope variability among mantle melts. Contrib to Mineral Petrol 133, 1–11. https://doi.org/10.1007/s004100050432.

Valley, J.W., Bindeman, I.N., Peck, W.H., 2003. Empirical calibration of oxygen isotope fractionation in zircon. Geochim. Cosmochim. Acta 67, 3257–3266. https://doi.org/10.1016/S0016-7037(00)00090-5.

Vezinet, A., Thomassot, E., Pearson, D.G., Stern, R.A., Luo, Y., Sarkar, C., 2019. Extreme $\delta^{18}O$ signatures in zircon from the Saglek Block (North Atlantic Craton) document reworking of mature supracrustal rocks as early as 3.5 Ga. Geology 47 (7), 605–608. https://doi.org/10.1130/g46086.1.

Vielzeuf, D., Veschambre, M., Brunet, F., 2005. Oxygen isotope heterogeneities and diffusion profile in composite metamorphic-magmatic garnets from the Pyrenees. Am. Mineral. 90, 463–472. https://doi.org/10.2138/am.2005.1576.

Whitney, D.L., Evans, B.W., 2010. Abbreviations for names of rock-forming minerals. Am. Mineral. 95, 185–187. https://doi.org/10.2138/am.2010.3371.

Wilde, S.A., Valley, J.W., Peck, W.H., Graham, C.M., 2001. Evidence form detrital zircons for the existence of continental crust and oceans 4.4 Ga ago. Nature 409, 175–178.

Williams, I.S., 1998. U–Th–Pb geochronology by ion microprobe. Rev. Econ. Geol. 7, 1–35.

Woodhead, J.D., Hellstrom, J., Hergt, J.M., et al., 2007. Isotopic and elemental imaging of geological materials by laser ablation inductively coupled plasma-mass spectrometry. Geostand Geoanalytical Res 31, 331–343.

Zheng, Y.-F., 1993a. Calculation of oxygen isotope fractionation in anhydrous silicate minerals. Geochim. Cosmochim. Acta 57, 1079–1091.

Zheng, Y.-F., 1993b. Calculation of oxygen isotope fractionation in hydroxyl-bearing silicates. Earth Planet. Sci. Lett. 120, 247–263.